Evolutionary dynamics of microbial communities in bioelectrochemical systems.

Lukasz Szydlowski[1*] | Anatoly Sorokin[23] | Olga Vasieva[4] |Veyacheslav Fedorovich[1] | Igor Goryanin[156]

[1] Okinawa Institute of Science and Technology, Japan

[*] Correspondence: Okinawa Institute of Science and Technology, Japan Email: lukasz.szydlowski@oist.jp ; Phone: +81-(0)98-982-3420

[2] Institute of Cell Biophysics, Russia

[3] Institute of Physics and Technology, Russia

[4] University of Liverpool, United Kingdom

[5] The School of Informatics, University of Edinburgh, United Kingdom

[6] Tianjin Institute for Industrial Biotechnology, China

SUMMARY

Bio-electrochemical systems can generate electricity by virtue of mature microbial consortia that gradually and spontaneously optimize performance. To understand selective enrichment of these electrogenic microbial communities, we set up five, 3-electrode reactors using the same inoculum derived from rice wash wastewater and incubated them under a range of applied potentials. We sampled reactors and extracted DNA from anodal, cathodal, and planktonic bacterial communities over 12 weeks. Using a custom-made bioinformatics pipeline, we combined 16S and metagenomic samples to analyze temporal changes in a community composition. We observed some genera that constituted a minor proportion of the initial inoculum, but that within weeks dominated the communities. Our study shows a correlation between community structure and applied potential. For instance, the abundance of *Geobacter* increased from 423-fold to 766-fold between -153 mV and 147 mV, respectively. Full metagenomic profiles of bacterial communities were obtained from reactors operating for 12 weeks. Functional analyses of metagenomes revealed metabolic changes between different species of the dominant genus, *Geobacter*, suggesting that optimal nutrient utilization at the lowest electrode potential is achieved via genome rearrangements and a strong inter-strain selection, as well as adjustment of the characteristic syntrophic relationships. Our observations reveal a certain degree of metabolic plasticity of electrochemically active bacteria and their communities in adaptation to adverse anodic and cathodic environments.

1 | INTRODUCTION

Bio-electrochemical Systems (BESs) refer to microbial communities that either generate electricity, as in Microbial Fuel Cells (MFCs) or utilize electricity, as in Microbial Electrolysis Cells (MECs) (Santoro *et al.*, 2017; Rittmann and Asce, 2017). BES is a well-known technology allowing simultaneous wastewater treatment and electricity production. BES performance depends on activities of electrode-associated bacteria (EAB) that form biofilms on anodal surfaces (e.g. Allen and Bennetto, 1993). Various factors account for EAB enrichment: organic substrates, pH, temperature, electrode composition, and electrical potential (Logan *et al.*, 2006; Aelterman *et al*., 2008; Torres *et al*., 2009; Dennis *et al*., 2016; Rittmann and Asce, 2017).

EAB reach maximum power density when reactors operate at near-neutral pH, at ambient temperatures (25-40^{o}C), and are fed with acetate. Although some studies indicate optimum electrode potentials at ca. 0.3 mV in comparison with a standard hydrogen electrode (SHE) (Aelterman *et al*., 2008), based upon thermodynamics of acetate consumption, others have found that the most efficient EAB prefer lower anode potentials (Torres *et al*., 2009). Microbial communities used to inoculate BESs were derived mainly from sludge from wastewater treatment plants (Torres *et al*., 2009; Ishii *et al*., 2013; Paitier *et al*., 2017), aquatic sediments (Holmes *et al*., 2004), biogas digestate (Daghio *et al*., 2015), and various environmental samples (e.g. Yates *et al*., 2012; Ieropoulos *et al*. 2010). EAB are abundant in many environments, such that virtually all environmental inocula can eventually give rise to stable EAB consortia within 60 days (Yates *et al*., 2012). However, further changes and details of community structure are not well understood.

Previous studies analyzed changes within microbial populations for up to several weeks (reviewed in Daghio *et al.*, 2015; Philips *et al*., 2015; Khater *et al*., 2017), and employed mainly 16S sequencing (Ishii *et al*., 2013; Ishii *et al.,* 2014; Dennis *et al*., 2016), Ribosomal Intergenic Spacer Analysis (RISA) (Paitier *et al*., 2017), or Denaturing Gradient Gel Electrophoresis (DGGE) (Beecroft *et al*., 2012). In another study,

community shifts were tracked during 90-days of operation (Beecroft *et al*., 2012). However, those reactors were fed with sucrose, which cannot be metabolized as efficiently (e.g. Schroder, 2007), as acetate (Bond *et al*., 2002; Bond and Lovley, 2003; Logan *et al*., 2006; Fedorovich *et al*., 2009; Daghio *et al*., 2015). Sucrose-fed systems developed fermentative communities that did not participate in electron transfer. Nevertheless, these population studies may significantly underestimate microbial diversity, with novel taxonomic groups not detected due to low compatibility with universal primers (e.g. Poretsky *et al*., 2014; Roselli *et al.,* 2016). Moreover, the type of inoculum also influences community development. In our previous work (Khylias *et al*., 2015), we showed that electrogenic communities derived from different sources exhibit different properties in terms of COD consumption, coulombic efficiencies, etc. Therefore, communities present in particular waste streams should already contain some electrogenic bacterial taxa. The minimal number of EAB is unknown and it remains unclear whether conclusions drawn by Yates et al. (2012) are valid for all inocula. Thus, complex studies, examining long-term community changes across a range of EAB-selective electrode potentials have not been attempted.

In this study, we investigated enrichment of EAB from rice wash inoculum in single-chamber, three-electrode BES. We normalized conditions among reactors utilizing acetate feeding to eliminate metabolic pathways other than that directly relevant to electrogenic respiration. We then applied a range of potentials, from 147 mV to -153 mV vs SHE on anodes and tracked compositional and functional changes in the resulting bacterial communities using detailed metagenomics.

2 | RESULTS

2.1 | Conditions within reactors

The single-chamber, 3-electrode BES reactors (M1-M4) were connected to a potentiostat to apply fixed

potentials (147 mV to -153 mV vs SHE) to the working electrodes (anodes). We also measured potentials observed (792 mV to 1182 mV vs SHE) on counter electrodes (cathodes). In addition, we prepared one reactor (M5) with only one set of electrodes to operate under open circuit potential (OCP) (Table 1). Our BESs were designed to develop electroactive biofilms, with high volume-to-electrode surface ratios in order to minimize nutrient limitations. Thus, after setting a constant potential, the potentiostat maintained current flow automatically and we did not measure current. One channel of the potentiostat, attached to reactor M3, exhibited an overload error after 8 weeks of operation, resulting in turbidity. This caused shift in community structure (Fig. S2); hence, we excluded this reactor from our analysis.

Reactor	Potential A (mV)	Potential C (mV)
M1	147	792
M2	47	972
M3*	-53	1082
M4	-153	1182
M5	0 to -333[a]	NA

Table 1. Potentials (measured with Ag/AgCl reference electrode in saturated KCl; +0.197 mV vs SHE) vs. SHE on anode **(A)** and cathode **(C)** of each reactor. [a)] Potentials measured in control (OCP) reactor after every 2 weeks. * Around week 8, we experienced technical fault in M3, resulting in overcharge of the reactor, which caused shift in the microbial community; results for this reactor are in Fig. S2 in supplementary material.

2.2 | Community analysis

Samples were collected every two weeks from anodes (M1-5A), cathodes (M1-4C) and planktonic (free swimming) fractions (M1-5P). Microscopic imaging (Fig.1) revealed that anodes from M1-M4 reactors developed communities that formed thick biofilms (Fig. 1a-c), and they were more abundantly populated than cathodes (Fig. 1e-g). No comparable community formed on electrode strips in M5 (Fig. 1d), due to its OCP mode. Negative charge accumulation on the electrode eventually inhibited microbial growth (Table 1).

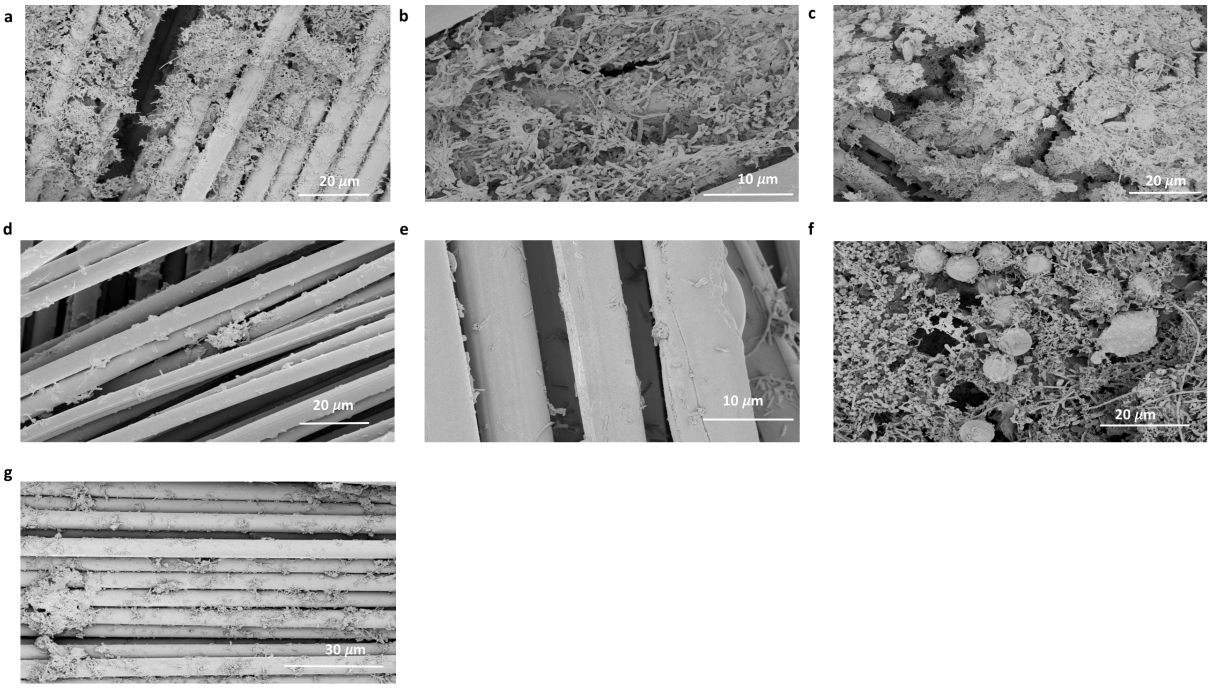

Fig. 1. SEM images of electrodes from a) M1A, b) M2A, c) M4A d) M5A e) M1C, f) M2C and g) M4C after 12 weeks of operation. Scale bars are included.

2.3 | Taxonomic analysis of anodes

We analyzed organismal abundances on each anode (Fig.2) during the 12-week operation, and compared them with initial community compositions (Table S2). Rice inoculum is nutrient-rich, although numbers of electrogenic taxa are very low, with *Geobacter* and *Shewanella* spp., two of the most efficient EABs, comprising less than 0.09% and 0.02% of the total communities, respectively. Enrichment data indicated that the abundance of *Geobacter* spp. rapidly increased over the first 6-8 weeks under poised anode potential (M1-4). Then, growth rates plateaued and the change in abundance of *Geobacter* after 12 weeks was 766-fold, 598-fold and 423-fold in M1A, M2A and M4A, respectively, whereas in M5A it only increased 1.2-fold. The relative abundance of *Geobacter* was significantly higher (ANOVA, $p < 0.05$) on M1A at 147 mV and decreased with decreasing potential. After 12 weeks of operation, the abundance of *Shewanella* remained unchanged in all reactors. Control reactor M5 showed an oscillating pattern of the most abundant genera *Methanosaeta*, *Methanobacterium*, and *Acinetobacter*, with an opposite oscillation pattern of *Prevotella* (Fig.2d), although the changes are not as significant as in the other reactors. With regard to generic abundance differences between the reactors, for M1A, *Geobacter* was the only genus with an abundance over 1%. M2A had 2 such genera (*Geobacter* and *Denitrovibrio*) and in reactor M4 and M5 anodes, the number of significantly abundant (i.e. > 1%) genera reached 10. Initially, 5 genera showed abundances >1%.

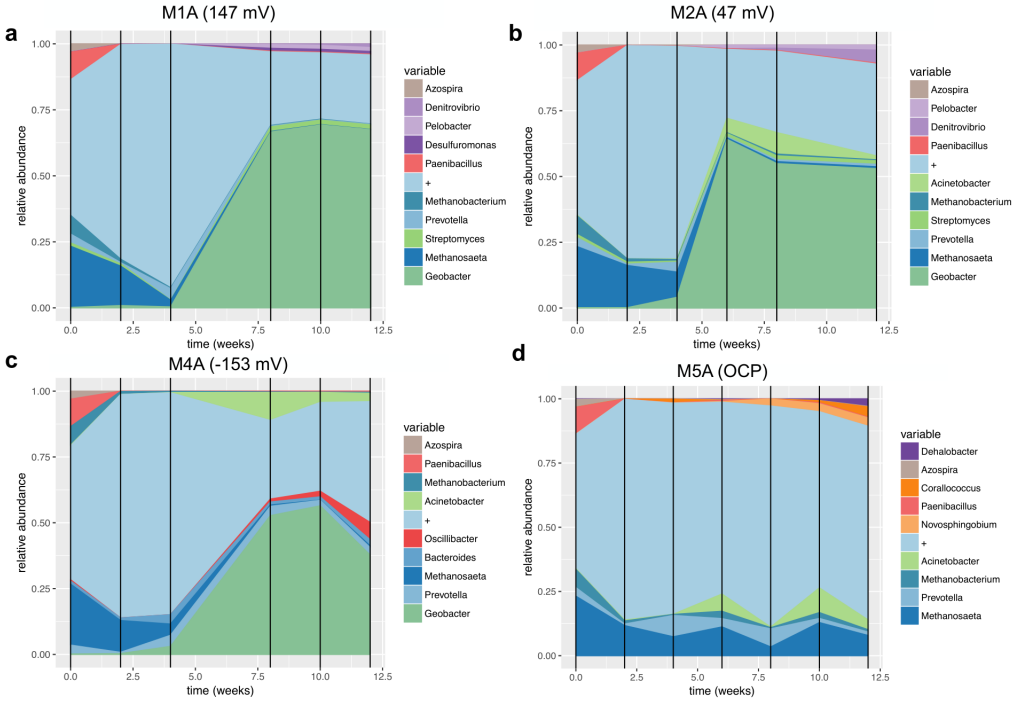

Fig. 2. Relative abundances of dominant genera collected from a) M1A, b) M2A, c) M4A and d) M5A during the experiment. Colors represent taxonomic groups, + - other organisms.

2.4 | Taxonomic analysis of cathodes

On the M1 and M2 cathodes, the most abundant organisms were methanogenic archaea (Fig.3a-b); however, a proportion of *Methanosaeta*, the most abundant methanogenic genus from the initial inoculum decreased during the course of the experiment, with subsequent growth of *Methanobacter* spp. The growth of the latter was in turn inversely correlated with that of *Methanoregula*. Contrarily, *Geobacter* was the most abundant genus on M4C, reaching a peak abundance of 16%, 12 weeks after inoculation, a level four times higher than that of the next most abundant genus, *Methanobacterium*

(Fig.3c). *Geobacter* remained scarce on the M1 and M2 cathodes (< 0.1%), not exceeding its abundance in the inoculum. On the M4 cathode, a rapid increase in its abundance after 10 weeks was accompanied by a concomitant decrease of *Acinetobacter* from 25% to 2.5% (Fig.3c).

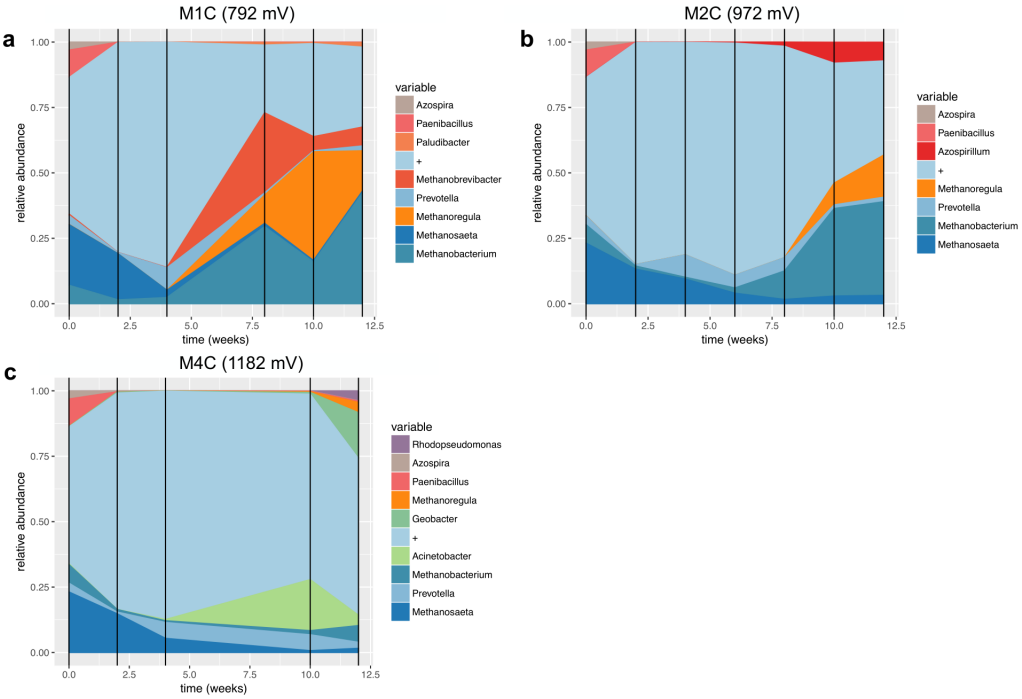

Fig. 3. Relative abundances of top genera collected a) M1C, b) M2C and c) M4C during the experiment. Colors represent taxonomic groups, + - other organisms.

2.5 | Taxonomic analysis of planktonic taxa

In the case of planktonic samples (Fig.4), a pattern of sudden growth around week 8, similar to that observed on M1A (although with much lower abundances) was observed with the genera, *Pelomonas*, *Paludibacter*, and *Bacteroides* in M1P. In all planktonic samples, *Methanosaeta*, the most abundant

112 genus in the inoculum (Table S1), decreased within the first weeks of operation, as did *Porphyromonas*
113 and *Azospirillum*. The proportion of *Pelomonas*, a genus comprising 0.01% of initial community, rose to
114 about 20% of the total planktonic community in M2. In M5P, abundances did not reflect the initial
115 community profile, as *Methanosaeta* decreased within 4 weeks from 24 % to ~1%, whereas *Azospirillum*
116 abundance reached ~25%.

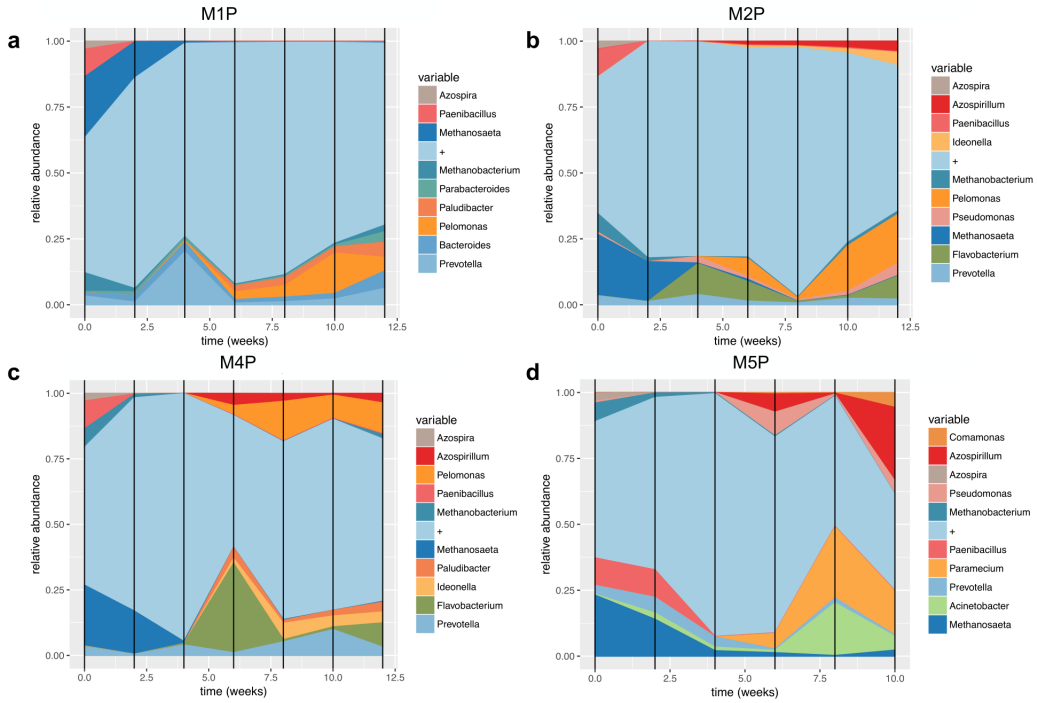

117

118 **Fig. 4**. Relative abundances of dominant genera collected from a) M1P b) M2P c) M4P and d) M5P during the
119 experiment. Colors represent taxonomic groups, + - other organisms.

120

121 ## 2.6 | Abundances of unclassified organisms

122 After 12 weeks of reactor operation, we compared the percentage of unclassified reads (at the

123 generic level) from each metagenome to that from the initial inoculum (Fig. 5). Results indicate
124 almost a 2-fold increase of unclassified taxa after 12 weeks in all sampled metagenomes, with
125 the highest being reported in M4P (34.9%), followed by M1P (31.9%) and M5P (30.0%), with
126 17% of unclassified genera in the initial inoculum.

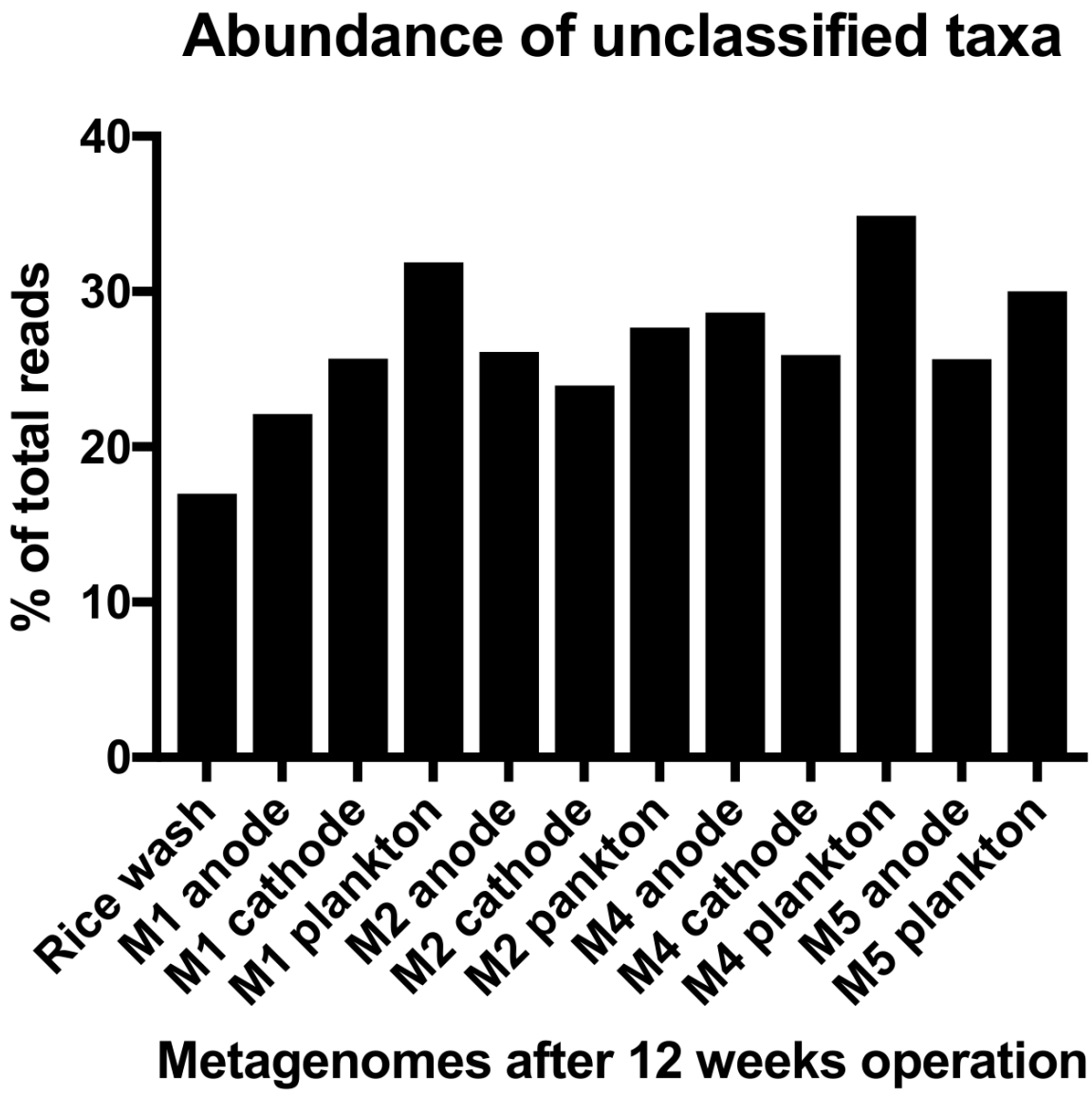

127

128 **Fig. 5**. Abundances of unclassified taxa (genera) after 12 weeks of operation, compared to the initial inoculum.

2.7 | Functional overview of metagenomes

Metagenomic analysis also revealed changes in abundances of functions mapped to the genomes and identified via PALADIN analysis, with mainly *Methanosaeta* functions being ranked in the top 200 by read count for initial communities and the M5 reactor (Tables S3 and S7, respectively). *Geobacter* functions dominated the ranked lists for M1, M2, and M4 reactors. We compared abundances in greater detail and ranked the top 200 *Geobacter* functions from each reactor (Supplementary tables S3-S7). The main abundance trend defined by the taxonomic analysis, correlates with the occurrence of *Geobacter* spp. in reactors, with counts for almost all mapped genes decreasing in the order M1, M4, M2, and M5 (the lowest). However, we also noticed changes in ranks (defined by a mapped-read count) of several *G. metallireducens* and *G. sulfurreducens* genes that may reflect changes in the proportion of these functionally significant genes in *Geobacteraceae* populations in different reactors. The rank of each gene was established in relation to the normalised abundance of its mapped reads (See Methods for a gene/function abundance calculation) for each species. The function with the highest number of mapped reads was assigned a rank of 1. Functions with lower numbers of mapped reads had lower ranks with larger assigned values. We conclude that the comparative rank measurement gives a better estimate of a functional genomic shift for a particular metagenome in relation to a reactor condition. Comparisons between ranks at M4A and M1A reveal that 14 genes have increased ranks in M4A, whereas those of 17 genes decreased (Table 2). An increase in rank order suggests potentially favourable genomic changes and may help to identify species-specific significant functions for specific reactor

151 conditions. The comparative nature of the analysis also helps to avoid biases caused by gene
152 length due to translation of the number of reads into a gene presentation ratio. Interestingly,
153 the results of such a comparison of *Geobacter* fractions at the M1 and M4 metagenomes (Table
154 2) revealed potential positive selection of bacteria for functions/genes involved in electrogenic
155 metabolism. Metagenomic changes in *G. sulfurreducens* were related to genes encoding ATP
156 synthase, NADH-quinone oxidoreductase, and the acetate utilization pathway, with 2-fold, 1.8-
157 fold, and 1.5-fold rank increases in M4A compared to M1A (Table 2a). Conversely, *G.*
158 *sulfurreducens* genes encoding ATPase (*prkA*), citramalate synthase (*cimA*), sodium symporter
159 (*aplC*), aldehyde dehydrogenase (*aldh*), and Fe-S binding protein increased 4-fold, 2.02-fold, 2-
160 fold, 1.52-fold, and 1.51-fold in rank in M1A, respectively (Table 2b). Changes in the *G.*
161 *metallireducens* metagenome included a wide range of functions involved in conductive pilin
162 assembly (*pilB*), flagella biosynthesis regulation (*fgrM*), pyruvate metabolism (*leuA*), and
163 electron transfer (*nuoB/C/G/L* and *por*), utilization of ammonia (*carb-1*) efflux pump (*cusA*), and
164 aspartokinase (*asd-1*) between 2-fold and 1.5-fold in M4A (Table 2a), whereas periplasmic Ni-Fe
165 dehydrogenase (*hybL*) and NADH-quinone oxidoreductase (*nuoD*) show 1.95 and 1.76 fold
166 increase in M1A (Table 2b).

167 a)

Hit ID	Protein	Organism	Rank	Rank change ratio
A0A0B5BDJ5	NADH-quinone oxidoreductase subunit H (EC 1.6.5.11)	*G. pickeringii*	M1A/148 M4A/**58**	2.55
nuoL-1 Gmet_3344	NADH dehydrogenase I, L subunit	*G. metallireducens*	M1A/73 M4A/**32**	2.28
nuoG-1 Q39QB3	NADH dehydrogenase I, G subunit	*G. metallireducens*	M1A/229 M4A/**105**	2.18

Q74GY2	ATP synthase subunit alpha (EC 3.6.3.14)	*G. sulfurreducens*	M1A/146 M4A/**70**	2.09
por Gmet_3419	Pyruvate-flavodoxin oxidoreductase (EC 1.2.7.-)	*G. metallireducens*	M1A/31 M4A/**15**	2.07
fgrM Gmet_3263	Flagellar biogenesis master sigma-54-dependent transcriptional regulator	*G. metallireducens*	M1A/117 M4A/**59**	1.98
Q74GY0	ATP synthase subunit beta (EC 3.6.3.14)	*G. sulfurreducens*	M1A/162 M4A/**82**	1.96
*pilB*_Q39XC1	Type IV pilus biogenesis ATPase PilB	*G. metallireducens*	M1A/355 M4A/**182**	1.95
carB-1 Gmet_1774	Carbamoyl-phosphate synthase large chain (EC 6.3.5.5)	*G. metallireducens*	M1A/124 M4A/**64**	1.94
leuA Gmet_1265	2-isopropylmalate synthase (EC 2.3.3.13)	*G. metallireducens*	M1A/175 M4A/**95**	1.84
Q746S4	NADH-quinone oxidoreductase subunit B/C/D (EC 1.6.5.11)	*G. sulfurreducens*	M1A/299 M4A/**168**	1.78
Q39QY3	Efflux pump, RND family, inner membrane protein	*G. metallireducens*	M1A/236 M4A/**139**	1.70
Q39UG5	Aspartokinase (EC 2.7.2.4)	*G. metallireducens*	M1A/322 M4A/**190**	1.69
ato-1 GSU0490	Succinyl:acetate coenzyme A transferase	*G. sulfurreducens*	M1A/150 M4A/**100**	1.50

b)

Gene ID	**Protein**	**Organism**	**Rank**	**Rank change ratio**
A0A0D5N7W1	ATPase	*G. sulfurreducens*	M1A/**2** M4A/8	-4.00
A0A0B5B7H3	Multiheme C-type cytochrome	*G. pickeringii*	M1A/**29** M4A/69	-2.38
A0A0B5BIF0	NADH-ubiquinone oxidoreductase subunit 3	*G. pickeringii*	M1A/**113** M4A/243	-2.15
*fabA/Z*_A5GFJ6	Beta-hydroxyacyl dehydratase, FabA/FabZ	*G. uraniireducens*	M1A/**108** M4A/232	-2.15
A0A0B5BC86	Multicopper oxidase	*G. pickeringii*	M1A/**120** M4A/253	-2.11

Q74C76	(R)-citramalate synthase (EC 2.3.1.182)	*G. sulfurreducens*	M1A/**39** M4A/79	-2.02
A0A1T4RHG2	Nif-specific regulatory protein	*G. thiogenes*	M1A/**61** M4A/122	-2.00
Q74AK2	Sodium/solute symporter family protein	*G. sulfurreducens*	M1A/**6** M4A/12	-2.00
A0A0B5BK17	Diguanylate cyclase	*G. pickeringii*	M1A/**57** M4A/113	-1.98
Q39QD0	Periplasmically oriented, membrane-bound [NiFe]-hydrogenase, large subunit	*G. metallireducens*	M1A/**102** M4A/199	-1.95
A0A0B5BAC1	Dihydrolipoyl dehydrogenase (EC 1.8.1.4)	*G. pickeringii*	M1A/**109** M4A/198	-1.82
A0A0B5BBC9	Type I citrate synthase (EC 2.3.3.1)	*G. pickeringii*	M1A/**149** M4A/269	-1.81
A0A0B5BJ81	NADH-quinone oxidoreductase subunit D (EC 1.6.5.11)	*G. metallireducens*	M1A/**25** M4A/44	-1.76
A0A0C1TL30	Flagellar basal body stator protein MotB	*G. soli*	M1A/**118** M4A/203	-1.72
*flgE/F*_A0A0B5BIQ7	Flagellar basal-body rod protein FlgF (Flagellar hook protein FlgE)	*G. pickeringii*	M1A/**127** M4A/206	-1.62
A0A0D5NB12	Aldehyde dehydrogenase	*G. sulfurreducens*	M1A/**171** M4A/260	-1.52
A0A0D5N6Q1	FeS-binding protein	*G. sulfurreducens*	M1A/**166** M4A/251	-1.51

Table 2. Rank increases of genes in a) M4A, b) M1A. Fold change ratio 1.5 was chosen as a threshold.

Genes from the *Geobacteraceae* (*G. pickeringii, G. uraniireducens, G. thiogenes,* and *G. soli*) mostly increased in rank in M1A, with outer membrane multiheme cytochrome c (*omc*), NADH-ubiquinone oxidoreductase (*nad3*), β-hydroxyacyl dehydratase (*fabA/Z*), multicopper oxidase (*ompB*), Nif-regulatory protein (*nifA*) exhibiting more than a 2-fold increase in rank, as well as dihydrolipoyl dehydrogenase (*lpdA*), type I citrate synthase (*gltA*), and flagellar components

(*motB*, *flgEF*), which exhibited 1.82, 1.81 and 1.7-fold shifts in rank, respectively (Table 2b). In M4A, a 2.55-fold rank increase was observed for the NADH quinone oxidoreductase gene (*nuoH*) from *G. pickeringii* (Table 2a).

In all planktonic samples, as well as in the initial community, top ranked genes are those involved in genome rearrangement (transposases, reverse transcriptases and endonucleases, see Tables S3-S7), which indicates selective pressure for adaptation to a more competitive environment. More detailed functional analysis of metagenomes collected in this study is described elsewhere (unpublished data).

3 | DISCUSSION

3.1 | Abundance of *Geobacter* spp. at anodes is directly proportional to the applied voltage

Geobacter is a well-characterized genus of EAB that populates BES anodes abundantly (Bond and Lovley, 2003). It can comprise ≤99% of bacterial communities isolated from BES electrodes operating at the lowest potential (Torres *et al*., 2009). However, our work indicates that the abundance of *Geobacter* increases at anodes with increasing applied potential, meaning that as the electrode potential increases, *Geobacter* competes more effectively with other genera in the community. In contrast, *Shewanella* did not increase in abundance under these conditions likely due to the fact that *Shewanella* primarily utilizes lactate as a carbon source (e.g. Kim *et al*., 1999; Pinchuk *et al.,* 2009).

Our abundance results contrast with those of Ishii *et al.* (2014), in which the highest abundance

of *Geobacter* spp. in acetate-fed, set-potential reactors was observed when anodes were held at -50 mV vs SHE. However, abundances from our study resemble those reported by Dennis *et al*. (2016). Also, the low initial population of *Geobacter* in the inoculum (see Table S2) may explain slower growth of *Geobacter* spp. at M4, compared to M1 and M2. Although periodic metagenomic sequencing reveals changes in the most abundant genera, it also indicates a large number of potentially undetected bacterial taxa. Changes in this community, as well as interactions among the most abundant EAB, will remain enigmatic, however, until genome assembly and isolation methods are improved to identify and characterize new strains.

3.2 | Presence of *Geobacter* spp. at cathodes

Apart from the *Geobacter* presence at anodes, *Geobacter* also dominated the M4 cathode community after 12 weeks, whereas it was scarcely present at other cathodes (0.06 and 0.07% in M1 and M2 cathodes, respectively) as well as at the M5 electrode (0.1%), being close to the inoculum abundance (0.08%). Such an increase in *Geobacter* spp. abundance in compartments with opposite conditions reflects its ability to both donate and accept electrons in association with electrodes (Holmes *et al*., 2004; Gregory *et al*., 2004). However, *Geobacter* was not found at cathodes in other studies (e.g. Daghio *et al*., 2015), which may reflect competition with different bacterial taxa, as well as differences in operating conditions, initial community structure, etc. Moreover, rank shifts of flagellar biosynthesis genes demonstrate ongoing colonization of new environmental niches by *Geobacter* spp. Recently, Rittmann and Asce (2017) concluded that the attribute to select the best-performing EAB is the lowest anode potential, but noted that such conditions are in fact stressful to the bacteria. Perhaps, the M4

cathode offered less deleterious conditions for *Geobacteriae* growth. The continuous decrease of methanogenic archaea at the M4 cathode may hint at competition for electrons with *Geobacter* spp., a known electrotroph (Strycharz *et al*., 2011). It might be tempting to suggest that incidental oxygen formation, due to the potential difference between M4 electrodes exceeded the potential difference at which electrolysis of water can occur (1.33 V vs 1.23 V). However, we did not observe bubble formation; therefore, the latter hypothesis may be discarded. Moreover, there are no abundance shifts due to oxygen stress between the M1 and M4 cathodic metagenomes (Table S2), which would certainly follow electrolysis by BES. There is also no evidence of rank shifts in genes involved in hydrogenotrophic methanogenesis, e.g., fumarate reductase, hydrogenase within. Microscopic observations (Fig. 1e-g) suggest some other relationship between *Geobacter* and methanogens in the cathodic community, e.g. via direct interspecies electron transfer (Lovley, 2017).

3.3 | Functional analysis and evidence of differential selection pressure on *Geobacter* at low electrode potentials.

We were intrigued by the dependence of observed genomic shifts in *Geobacter* metabolic functions on reactor conditions. The changes themselves, relevant to main pathways of electrogenic organisms in MFC, suggest that bacterial genomes evolve rapidly due to metabolic competition. Acetate metabolism is central to metabolism of *G. sulfurreducens* under electrogenic conditions (Bond and Lovley, 2003; Ieropoulos *et al*., 2010). This metabolic feature allows these bacteria to dominate anodic communities if acetate is provided or generated by other members of the syntrophic bacterial community (e.g. *G. metallireducens).* Interestingly,

239 *G. sulfurreducens* functions required for acetate utilization (*ato*) were the only ones from this
240 species that strongly changed rank at lower anodic potential (M4) (Table 2a), with aldehyde
241 dehydrogenase rank decreasing (Table 2b). Acetate utilization by *G. sulfurreducens* may be
242 supported by a syntrophic association with *Pelobacter* spp. (Sreshtha *et al*., 2013), and
243 enrichment of this genus was observed on anodes M1 and M2 (Fig. 2a-b). Though acetate was
244 provided in the medium, local interactions between bacteria and bacterial clusters may be
245 significant. Sequences corresponding to ATP synthase subunits also increased in abundance in
246 M4A, with a 4-fold decrease in ATPase (Table 2), suggesting higher pressure for energy
247 generation.

248 At the same time, adaptation and evolution of highly electrogenic *G. metallireducens* at M4
249 seems to proceed due to a requirement for conductive pili, respiratory NADH dehydrogenases,
250 and pyruvate metabolism, which increase in rank at M4A (Table 2a). NuoL, for which
251 metagenomic rank changed most at the M4 anode compared to M1A, is responsible for the
252 reverse electron transfer and H^+/e^- stoichiometry (Steimle *et al.,* 2011), which may be
253 important for balancing electron flow between NAD+ and ferredoxin pools. PilB is an ATPase
254 required for polymerization of conductive e-pili (McCallum *et al.*, 2017), and *pilB* mutants are
255 reported to generate lower current and form thinner biofilms (Steidl *et al.,* 2016). Additionally,
256 it was observed by Ishii *et al*. (2018) that *pilA* expression increased at lower surface potential.
257 Change in *pilB expression* has not been reported there, although it could be a result of a
258 normalization procedure: with an increase in a number of DNA reads, change in number of RNA
259 reads/expression could not be observed.
260 Flagellar response regulator (*fgrM*), which increased in rank in M4A, regulates flagellar growth,

261 a feature known in *G. metallireducens* when grown with an insoluble Fe(III) source (Ueki *et al.*,
262 2012). This feature corresponds to increased motility of cells when Fe(III) sources are scattered.
263 Cells can store electrons in their numerous cytochromes, acting as capacitors, so that they can
264 discharge them upon the next available Fe(III) cluster. Similarly, lower surface potential of
265 anode in M4A could lead to formation of dispersed local spots for electron release. Thus, *G.*
266 *metallireducens* cells with regulated expression of flagella proteins could possess higher and
267 more ordered motility, which, together with the higher capacity to polymerize e-pili by PilB,
268 should give them advantage over competitors.

269 The study shows a decrease in rank of genes belonging to other taxa (*G. pickeringii, G.*
270 *uraniireducens, G. thiogenes* and *G. soli*) at lower surface potential (Table 2b). Citrate synthase
271 (*G. pickeringii*), a proposed indicator of Geobacteraceae metabolic activity (Holmes *et al.,* 2005)
272 decreased almost 2-fold at M4A. Also, genes encoding components of EET are lower in rank at
273 M4A (Table 2b). This correlates with the limited capacity of these Geobacteraceae to adapt to
274 low surface potential, as their electrochemical activity was reported for rather more positive
275 redox potentials (Ishii *et al.,* 2018).

276 Certainly, gene abundance cannot be taken as an unequivocal reflection of activity levels of
277 relevant functions in bacterial metabolism under different conditions. However, we suggest
278 that genomic rearrangements represent responses to specific functional requirements. Genes
279 may be retained or even propagate in a population if they enhance organismal fitness.
280 Increasing abundances of bacterial strains bearing advantageous genes may also explain the
281 observed phenomenon. As shown in the case of *pilB* gene, analysis of gene ranks derived from

metagenomics analysis can complement expression studies.

3.4 | The importance of unknown organisms in a functional overview of these metagenomes

The presence of unclassified taxa indicates an increase in abundance of unknown organisms upon inoculation into BES reactors. Our results (Fig. 4) do not align with previous work (Ishii *et al.,* 2014), in which unclassified taxa in the inoculum contained comparable numbers of unclassified reads, but only several percent of unclassified organisms were sampled from the electrodes. The discrepancy between the two studies may be due to the difference in sampling and sequencing methods. The former study employed only 16S samples, whereas we compared Illumina MiSeq whole metagenomic reads. Such discrepancies were also reported in a later study by Ishii et al. (2018), where lower diversity was reported in the same samples when only 16S analysis was employed. The abundance of novel unidentified organisms suggests the existence of novel electrogenic microorganisms. Such organisms may not be as efficient in EET as *Geobacter spp*.; hence the term “weak electricigens” (Doyle and Marsili, 2018), but they may nonetheless provide useful insight into the divergence of EET mechanisms. However, since their increases do not follow electrode potential, the presence of so many unclassified organisms, may be more related to the inoculum than to reactor conditions.

4 | EXPERIMENTAL PROCEDURES

4.1 | Reactor setup and operating conditions

Four reactors (M1-4) were designed as follows: 1.2L chamber with an anode consisting of 6 carbon-fiber

strips (Zoltec) 3x10 cm connected with titanium wire (Kojundo chemical laboratory), a cathode consisting of 6 carbon-fiber strips (Zoltec) 3x10 cm connected with titanium wire, and a reference electrode (Radiometer Analytical, Hach). Additionally, one control reactor (M5) consisted only of one set of 6 carbon-fiber strips (Zoltec) 3x10 cm connected with titanium wire and reference electrode (Radiometer Analytical, Hach), and was operated in open circuit mode (see Fig.S1 for schematic view). A four-channel potentiostat (UniChem) was connected to each reactor with stainless steel clips and potential differences of 147 mV, 47 mV, -53 mV and -153 mV (vs SHE) were applied to anodes M 1-4A, respectively. Each reactor was inoculated with rice wash water (1.2L) and incubated for 2 weeks at room temperature (23^{o} C), after which the liquid was replaced with an equal volume of the following medium: 0.05 M phosphate buffer (pH 6), 200 mg/L $CaCl_2 \bullet 2H_2O$, 250 mg/L $MgCl_2 \bullet 6H_2O$, 500 mg/L NH_4Cl, sodium acetate 2g COD/L (Fedorovich *et al*., 2009). COD concentration was measured using a Hach COD kit (Hach, USA). The medium was replaced 6 times at 2-week intervals, yielding a total operating time of 12 weeks. Additionally, 50 mL of liquid fraction and one strip of each electrode (1x A and 1x C from M1-4 and 1x A from M5) were collected with every change of medium. These were used for DNA extraction and SEM analysis.

4.2 | Microscopic imaging

Samples for microscopic imaging were taken simultaneously with the DNA samples and processed with osmium, as follows (Fischer *et al*., 2012): upon removal from the anode compartment, the samples were immediately cut by knife, and fixed by 1%Osmium diluted with 0.2M Cacodylate (Wako) buffer 30min. The samples were then washed three times with RQ water and dehydrated stepwise with a graded series of ethanol solutions (70, 80, 90, 95 and three times 100%). The electrode samples were finally critical-point dried with tert-butyl ethanol and sputter coated with a thin layer of gold. The samples were analyzed by a scanning electron microscopy (SEM) (JSM-7900F JEOL).

4.3 | DNA extraction and library preparation

DNA was extracted using TRIzol (Life Technologies) and additional samples were subjected to Maxwell extraction (GMO purefood kit, Maxwell) using an automated RSC system (Promega). Samples with sufficient amounts of DNA were subjected to Illumina sequencing (48). Remaining samples (32) were subjected to 16S sequencing. DNA libraries were constructed using Nextera XT kit (Illumina) and sequencing was performed on MiSeq platform (Illumina, San-Diego, CA, USA). Samples were uploaded to MG-RAST (mgp81854 for 16S, mgp82844 for metagenomes). We were unable to collect data from 3 cathodal samples (see Table S1).

4.4 | Bioinformatic analysis

Whole-genome sequences and 16S sequences were analyzed using a custom-developed pipeline, as described elsewhere (Orakov *et al*., 2017), which carried out taxonomic analysis using Kaiju (Menzel and Krogh, 2016), as well as functional analysis using PALADIN (only applicable to metagenomes) (Westbrook *et al*., 2017). Results of PALADIN analysis for anodes M1 and M4 can be found in the Supplementary material (Table S3). Compositional analysis of communities was performed in R version 1.4.0 (van den Boogaart *et al*., 2018) with package compositions (van den Boogaart and Tolosana-Delgado, 2008). Relative abundance was represented as composition with absolute geometry (rcomp). To combine 16S and metagenomic sequences, datasets from Kaiju and MG-RAST were manually curated (a more detailed description can be found at https://github.com/lptolik/ASAR). One-way ANOVA was conducted to determine the significance of differences in abundance of *Geobacter* between M1A, M2A and M4A for the period between week 8 and 12. For visualization purposes, the five most abundant genera in the inoculum and five most abundant genera in Week 12 were selected. All other genera were included in the “Other” group. The R script employed is described in Orakov *et al*. (2017).

ACKNOWLEDGEMENTS

This research was supported by Okinawa Institute of Science and Technology Graduate University. We thank Dr. Larisa Kiseleva for collecting electrode and plankton samples and Dr. Toshio Sasaki for preparing SEM specimens.

CONFLICT OF INTEREST

The authors declare no conflict of interest.

REFERENCES

Aelterman, P., Freguia, S., Keller, J., Verstraete, W. and Rabaey, K. (2008) The anode potential regulates bacterial activity in microbial fuel cells. *Applied microbiology and biotechnology*, **78**, 409–418.

Allen, R. M. and Bennetto, H. P. (1993) Microbial fuel cells: Electricity production from carbohydrates. *Applied Biochemistry and Biotechnology*, **39**, 27–40.

Beecroft, N. J., Zhao, F., Varcoe, J. R., Slade, R. C. T., Thumser, A. E. and Avignone-rossa, C. (2012) Dynamic changes in the microbial community composition in microbial fuel cells fed with sucrose. *Applied Microbiology and Biotechnology,* **93** 423–437.

Bond, D. R., Holmes, D. E., Tender, L. M. and Lovley, D. R. (2002) Electrode-Reducing Microorganisms That Harvest Energy from Marine Sediments. *Science*, **295**, 483–485.

Bond, D. R. and Lovley, D. R. (2003) Electricity Production by *Geobacter sulfurreducens* Attached to Electrodes Electricity Production by *Geobacter sulfurreducens* Attached to Electrodes. *Applied and Environmental Microbiology*, **69**, 1548–1555.

van den Boogaart, K., Tolosana, R. and Bren, M. (2018) Compositions: Compositional data analysis. r-package version 1.40–1.

van den Boogaart, K. G. and Tolosana-Delgado, R. (2008) "compositions": A unified R package to analyze compositional data. *Computers & Geosciences*, **34**, 320–338.

Brooks, J. P., Edwards, D. J., Harwich, M. D., Rivera, M. C., Fettweis, J. M., Serrano, M. G., Reris, R. A., Sheth, N. U., Huang, B., Girerd, P., Strauss, J. F., Jefferson, K. K. and Buck, G. A. (2015) The truth about metagenomics: Quantifying and counteracting bias in 16S rRNA studies Ecological and evolutionary microbiology. *BMC Microbiology*, **15**, 1–14.

Cord-Ruwisch, R., Lovley, D. R., Schink, B. (1998). Growth of Geobacter sulfurreducens with acetate in syntrophic cooperation with hydrogen-oxidizing anaerobic partners. Applied and Environmental Microbiology, 64(6), 2232–2236.

Daghio, M., Gandolfi, I., Bestetti, G., Franzetti, A., Guerrini, E. and Cristiani, P. (2015) Anodic and cathodic microbial communities in single chamber microbial fuel cells. *New Biotechnology*, **32**, 79–84.

Dennis, P. G., Virdis, B., Vanwonterghem, I., Hassan, A., Hugenholtz, P., Tyson, G. W. and Rabaey, K. (2016) Anode potential influences the structure and function of anodic electrode and electrolyte-associated microbiomes. *Scientific Reports*,**6**, 1–11.

Doyle, L. E., & Marsili, E. (2018). Weak electricigens: A new avenue for bioelectrochemical research. *Bioresource Technology*, 258, 354–364.

Dupuis, A., Peinnequin, A., Darrouzet, E., Lunardi, J. (1997). Genetic disruption of the respiratory NADH-ubiquinone reductase of Rhodobacter capsulatus leads to an unexpected photosynthesis-negative phenotype. FEMS Microbiology Letters, 148(1), 107–114.

Fedorovich, V., Knighton, M. C., Pagaling, E., Ward, F. B., Free, A. and Goryanin, I. (2009) Novel electrochemically active bac-

terium phylogenetically related to *Arcobacter butzleri*, isolated from a microbial fuel cell. *Applied and Environmental Microbiology*, **75**, 7326–7334.

Fischer, E. R., Hansen, B. T., Nair, V., Hoyt, F. H. and Dorward, D. W. (2012) Scanning Electron Microscopy. *Current Protocols in Microbiology*, 1–16.

Gregory, K. B., Bond, D. R. and Lovley, D. R. (2004) Graphite electrodes as electron donors for anaerobic respiration. *Environmental Microbiology*, **6**, 596–604.

Holmes, D. E., Bond, D. R., O'Neil, R. A., Reimers, C. E., Tender, L. R. and Lovley, D. R. (2004) Microbial communities associated with electrodes harvesting electricity from a variety of aquatic sediments. *Microbial Ecology*, **48**, 178–190.

Ieropoulos, I., Winfield, J. and Greenman, J. (2010) Effects of flow-rate, inoculum and time on the internal resistance of microbial fuel cells. *Bioresource Technology*, **101**, 3520–3525.

Ishii, S., Suzuki, S., Norden-Krichmar, T. M., Tenney, A., Chain, P. S. G., Scholz, M. B., Nealson, K. H. and Bretschger, O. (2013) A novel metatransctiptomic approach to identify gene expression dynamics during extracellular electron transfer. *Nature Communications,* **4:1601,** 1–10.

Ishii, S., Suzuki, S., Norden-Krichmar, T. M., Phan, T., Wanger, G., Nealson, K. H., … Bretschger, O. (2014). Microbial population and functional dynamics associated with surface potential and carbon metabolism. *ISME Journal*, 8(5), 963–978.

Ishii, S., Suzuki, S., Tenney, A., Nealson, K. H., & Bretschger, O. (2018). Comparative metatranscriptomics reveals extracellular electron transfer pathways conferring microbial adaptivity to surface redox potential changes. *ISME Journal*, 12(12), 2844–2863.

Kim, H. J., Hyun, M. S., Chang, I. S., & Kim, B. H. (1999). A microbial fuel cell type lactate biosensor using a metal-reducing bacterium, *Shewanella putrefaciens. Journal of Microbiology and Biotechnology*, 9(3), 365-367.

Pinchuk, G. E., Rodionov, D. A., Yang, C., Li, X., Osterman, A. L., Dervyn, E., … Beliaev, A. S. (2009). Genomic reconstruction of *Shewanella oneidensis* MR-1 metabolism reveals a previously uncharacterized machinery for lactate utilization. *Proceedings of the National Academy of Sciences*, 106(8), 2874–2879.

Khater, D. Z., El-khatib, K. M. and Hassan, H. M. (2017) Microbial diversity structure in acetate single chamber microbial fuel cell for electricity generation. *Journal of Genetic Engineering and Biotechnology*, **15**, 127–137.

Logan, B. E., Hamelers, B., Rozendal, R., Schroder, U., Keller, J., Freguia, S., Aelterman, P., Verstraete, W. and Rabaey, K. (2006) Microbial Fuel Cells : Methodology and Technology. *Environmental Science and* Technology, **40** (17), 5181–5192.

Lovley, D. R. (2017). Syntrophy Goes Electric: Direct Interspecies Electron Transfer. *Annual Review of Microbiology*, 71(1), 643-664.

McCallum, M., Tammam, S., Khan, A., Burrows, L. L., & Lynne Howell, P. (2017). The molecular mechanism of the type IVa pilus

motors. *Nature Communications*, 8(May), 1–10.

Menzel, P. and Krogh, A. (2016) Kaiju: Fast and sensitive taxonomic classification for metagenomics. *Nature communications*, **7**, 1–9.

Orakov, A., Sakenova, N., Sorokin, A. and Goryanin, I. (2017) ASAR: visual analysis of metagenomes in R. *Bioinformatics*, 0–0.

Orellana, Roberto (2014). "PHYSIOLOGICAL MODELS OF GEOBACTER SULFURREDUCENS AND DESULFOBACTER POSTGATEI TO UNDERSTAND URANIUM REMEDIATION IN SUBSURFACE SYSTEMS" (2014). *Doctoral Dissertations.*

Paitier, A., Godain, A., Lyon, D., Haddour, N., Vogel, T. M. and Monier, J.-M. (2017) Biosensors and Bioelectronics Microbial fuel cell anodic microbial population dynamics during MFC start-up. *Biosensors and Bioelectronics*, **92**,357–363.

Philips, J., Verbeeck, K., Rabaey, K. and Arends, J. (2015) Electron transfer mechanism in biofilms. In *Microbial Electrochemical and Fuel Cells Fundamentals and Applications* (eds. K. Scott and E. H. Yu), chap. 3, 113–169. Cambridge: Woodhead Publishing (Elsevier), first edn.

Poretsky, R., Rodriguez-r, L. M., Luo, C., Tsementzi, D. and Konstantinidis, K. T. (2014) Strengths and Limitations of 16S rRNA Gene Amplicon Sequencing in Revealing Temporal Microbial Community Dynamics. *PLOS One,* **9**(4), e93827.

Rosselli, R., Romoli, O., Vitulo, N., Vezzi, A., Campanaro, S., De Pascale, F., … Squartini, A. (2016). Direct 16S rRNA-seq from bacterial communities: A PCR-independent approach to simultaneously assess microbial diversity and functional activity potential of each taxon. *Scientific Reports*, **6**(February), 1–12.

Rittmann, B. E. and Asce, D. M. (2017) Ironies in Microbial Electrochemistry. *Journal of Environmental Engineering*, **143**, 1–7.

Santoro, C., Arbizzani, C., Erable, B., Ieropoulos, I. (2017). Microbial fuel cells: From fundamentals to applications. A review. Journal of Power Sources, 356, 225–244.

Schroder, U. (2007) Anodic electron transfer mechanisms in microbial fuel cells and their energy efficiency. *Physical Chemistry Chemical Physics*, **9**, 2619–2629.

Shrestha, P. M., Rotaru, A. E., Summers, Z. M., Shrestha, M., Liu, F., Lovley, D. R. (2013). Transcriptomic and genetic analysis of direct interspecies electron transfer. *Applied and Environmental Microbiology*, 79(7), 2397–2404.

Shrestha, P. M. and Rotaru, A. E. (2014) Plugging in or going wireless: Strategies for interspecies electron transfer. *Frontiers in Microbiology*, **5**, 1–8.

Steidl, R. J., Lampa-Pastirk, S., & Reguera, G. (2016). Mechanistic stratification in electroactive biofilms of Geobacter sulfurreducens mediated by pilus nanowires. *Nature Communications*, 7.

Steimle, S., Bajzath, C., Dorner, K., Schulte, M., Bothe, V., Friedrich, T. (2011). Role of subunit NuoL for proton translocation by respiratory complex I. *Biochemistry*, 50(16), 3386–3393.

Torres, C. I., Krajmalnik-Brown, R., Parameswaran, P., Marcus, A. K., Wanger, G., Gorby, Y. A. and Rittmann, B. E. (2009)

444 Selecting Anode-Respiring Bacteria Based on Anode Potential: Phylogenetic, Electrochemical, and Microscopic Characterization.
445 *Environ. Sci. Technol.*, **43**, 9519–9524.

446 Westbrook, A., Ramsdell, J., Schuelke, T., Normington, L., Bergeron, R. D., Thomas, W. K. and MacManes, M. D. (2017) PALADIN:
447 Protein alignment for functional profiling whole metagenome shotgun data. *Bioinformatics*, **33**, 1473–1478.

448 Yates, M. D., Kiely, P. D., Call, D. F., Rismani-Yazdi, H., Bibby, K., Peccia, J., Regan, J. M. and Logan, B. E. (2012) Convergent
449 development of anodic bacterial communities in microbial fuel cells. *ISME Journal*, **6**, 2002–2013.